Macromolecules

pubs.acs.org/Macromolecules Article

# Control of Solution Phase Behavior through Block–Random Copolymer Sequence

Lauren W. Taylor, Rodney D. Priestley,* and Richard A. Register*

Cite This: *Macromolecules* 2024, 57, 916–925 Read Online

ACCESS | Metrics & More | Article Recommendations | Supporting Information



**ABSTRACT:** The phase behavior of polymers in solution is of both fundamental and practical interest. Previous work using coarse-grained molecular simulations suggests that the critical temperature ($T_c$) of macromolecules in solution can be controlled by the monomer sequence. Here, we experimentally investigated the solution phase behavior of a series of styrene–isoprene copolymers in both styrene- and isoprene-selective solvents. Across the series, the copolymers had a similar overall composition and molecular weight but subtle changes in the monomer sequence obtained by systematically placing a short homopolymer block of either polystyrene or polyisoprene at the end or the center of an otherwise random styrene–isoprene copolymer chain. Compared with a fully random copolymer, sequences that microphase-separate to form starlike or crew-cut micelles produce a lower $T_c$. Conversely, sequences that do not form micelles exhibit a higher $T_c$. Through a delicate balance of solvent/polymer compatibility, we demonstrate the spontaneous and thermoreversible formation of unusually large (aggregation number, ~1000), stable crew-cut micelles. Despite the unusual structure, the thermodynamics of formation of these crew-cut micelles is similar to that of starlike block copolymer micelles.

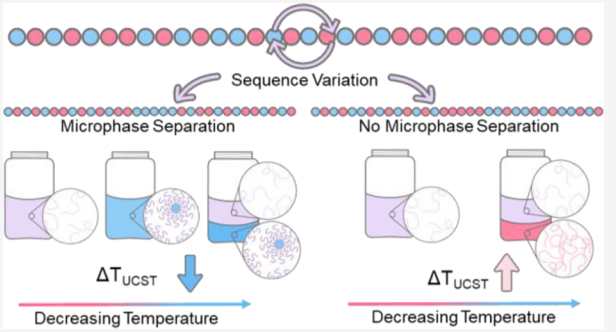


## INTRODUCTION

Phase separation is crucial to material function in both synthetic and biological soft matter. In synthetic systems, phase separation processes are used to make complex structures such as porous polymer membranes[1] and structured colloids.[2,3] In biological systems, liquid–liquid phase separation in aqueous solutions of intrinsically disordered proteins (IDPs) is the underlying mechanism for the formation of biological condensates within cells.[4,5] To prompt these microphase and macrophase separations, both systems utilize environmental stimuli such as temperature,[6] solution composition,[7,8] or light,[9,10] and precise control of these phase transitions could enable the development of smart materials for environmental and medical applications.[11−13] Therefore, significant effort has been spent on understanding how the material structure affects phase behavior. In particular, responses to temperature have been extensively studied due to the ease of applying the stimulus.[14]

In many polymer solutions, macrophase separation is characterized by upper critical solution temperature (UCST) behavior.[15,16] In these systems, the compatibility between the polymer and the solvent decreases with a decrease in temperature, causing phase separation upon cooling. The onset of phase separation is characterized by the formation of polymer aggregates that are large enough to scatter light. The phase transition occurs at the cloud point temperature ($T_{cp}$) and is easily measured by solution turbidity.[17] Furthermore, $T_{cp}$ varies with the polymer concentration. The upper critical solution temperature ($T_c$) is the temperature above which the polymer solution is single-phase for any concentration of the polymer.[18] Polymer solutions can also microphase-separate to form self-assembled structures such as spherical micelles, vesicles, rods, and lamellae.[19,20] The onset of micelle formation through changes in the thermodynamic state (temperature, polymer concentration, and pressure) produces a change in the average particle size, and thus the diffusion coefficient, that can be measured with dynamic light scattering (DLS).[21] Aqueous solutions that can both micro- and macrophase-separate through temperature variation have been demonstrated for several polymers containing poly(ethylene oxide) blocks,[22−24] and this dual behavior has previously been attributed to the unique solvation properties of water.[25] However, recent Monte Carlo simulations of polymers composed of solvophilic and solvophobic beads indicate that both phenomena should be accessible for carefully selected copolymer sequences regardless of the choice of solvent,[26] although such behavior has yet to be observed experimentally in nonaqueous solutions.

**Received:** October 13, 2023
**Revised:** December 21, 2023
**Accepted:** December 27, 2023
**Published:** January 16, 2024

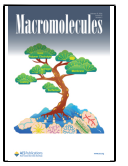





https://doi.org/10.1021/acs.macromol.3c02111
*Macromolecules* 2024, 57, 916–925

Previous works have reported monomer chemistry,[27] copolymer composition,[28,29] polymer architecture,[30,31] molecular weight,[32,33] and solvent quality[7,8] as routes to tailor the thermoresponsive behavior of polymers. However, in applications such as drug delivery, the solvent quality cannot be altered, and altering material chemistry can affect other key functionalities such as biocompatibility and viscosity. Biological systems are believed to use proteins with a similar amino acid composition but a varying sequence to control phase separation,[34] and experimental work has shown that point mutations in IDPs can suppress liquid−liquid phase separation.[35] In synthetic macromolecular systems, even alternating vs random copolymers of the same composition have been shown to differ in phase behavior.[36] Simulations of macromolecules have explored the influence of the sequence on phase behavior in detail.[37−39] Statt et al. used coarse-grained molecular simulations to model IDPs using solvophilic and solvophobic segmental beads.[38] These studies demonstrated that small changes in the bead sequence at a fixed chain composition can profoundly impact liquid−liquid phase separation. Furthermore, the authors found that the beads at the end of the chain had a stronger impact on phase behavior than the sequence changes in the center of the chain.

Here, we show experimentally that small modifications in the copolymer sequence can effectively modulate phase behavior. "Block−random" styrene−isoprene copolymers were synthesized with blocks (5−10 wt % of the total polymer chain) of a polystyrene (PS) or polyisoprene (PI) homopolymer in the middle or at the end of a random copolymer chain while keeping the overall styrene:isoprene ratio fixed at 50/50 (w/w). The phase behavior was explored in two selective solvents, *n*-hexane and *N*,*N*′-dimethylacetamide (DMAc), which preferentially dissolve PI and PS, respectively. The $T_c$ for each block−random polymer was measured by solution turbidity and compared with fully random styrene−isoprene copolymers (PSRPI) with the same overall monomer composition. Additionally, microphase separation into spherical micelles was characterized using dynamic light scattering (DLS). We find that when a polymer sequence forms micelles, $T_c$ decreases compared with a PSRPI copolymer of the same composition. When a block−random polymer does not undergo microphase separation, $T_c$ increases compared to that of a PSRPI copolymer of the same composition. Therefore, $T_c$ can be controlled by the careful selection of block and solvent compatibilities. Furthermore, we demonstrate a single system that undergoes both micro- and macrophase separation by varying temperature, a phenomenon previously believed to be unique to aqueous solutions. Finally, we show spontaneous and thermoreversible formation of very large (aggregation number, ∼1000) but stable crew-cut micelles, a structure typically achievable only through removal of a mutual solvent.[40,41] These findings provide insights toward designing new thermoresponsive materials with control over both micro- and macrophase separation, enabling additional functionalities.

## EXPERIMENTAL SECTION

**Polymer Synthesis.** Styrene−isoprene copolymers were synthesized via anionic polymerization, as shown in Figure S1. A glass reaction vessel was charged with *tert*-butyllithium (1.7 M in pentane, Sigma-Aldrich) in a nitrogen-filled glovebox (MBRAUN UNIlab, <0.1 ppm $H_2O$ and $O_2$). A 50/50 (v/v) mixture of cyclohexane (≥99.9%, Sigma-Aldrich) and triethylamine (≥99.5%, Sigma-Aldrich) was used as the reaction solvent. The mixed solvent was stirred over the red adduct of *n*-butyllithium (2.0 M in cyclohexane, Sigma-Aldrich) and 1,1-diphenylethylene (97%, Sigma-Aldrich), degassed by freeze−pump−thaw (FPT) cycles, and vacuum transferred directly into the reaction vessel. The styrene monomer (≥99%, Sigma-Aldrich) was stirred over *n*-butylethylmagnesium (0.9 M in heptane, Acros Organics), and the isoprene monomer (99%, Sigma-Aldrich) was stirred over *n*-butyllithium. Monomers were degassed via FPT before being vacuum transferred into the reaction vessel. Each block was polymerized for 2 h at 30 °C to ensure essentially complete monomer conversion and good control of the polymer sequence. Isopropanol (ACS, LabChem) was degassed via FPT and vacuum transferred to the reaction flask to terminate the copolymers. Polymers were precipitated into cold methanol (ACS, Fisher Chemical) and dried in a vacuum oven at 65 °C for 4 days.

**Molecular Characterization.** The copolymer composition and polyisoprene microstructure were determined by $^1$H nuclear magnetic resonance (NMR) spectroscopy. Polymers were dissolved at 5 mg/mL in deuterated chloroform (99.8%, Cambridge Isotope Laboratories, Inc.), and spectra were collected on a Bruker Avance III 500 MHz spectrometer. All NMR data analysis was performed with MestReNova software (Mestrelab Research).

The weight-average molecular weight ($M_w$), number-average molecular weight ($M_n$), and dispersity ($Đ$) were characterized by gel permeation chromatography (GPC) using two 30 cm Agilent PLgel 5 μm Mixed-C columns operating at 35 °C, a Wyatt Optilab T-rEX differential refractive index (DRI) detector (25 °C, 658 nm wavelength), and a miniDAWN TREOS three-angle light scattering instrument (ambient temperature, 658 nm). Tetrahydrofuran (inhibitor-free HPLC, Sigma-Aldrich) was used as the mobile phase. $M_w$ was measured by using light scattering. The d*n*/d*c* for each polymer was calculated using a weighted average for polystyrene (0.189 mL/g) and polyisoprene of similar microstructures (0.125 mL/g) using the polymer composition determined from $^1$H NMR.[42] The DRI elution time was calibrated with narrow-distribution polystyrene standards, from which $Đ$ was determined. Finally, $M_n$ was calculated as $M_n = M_w/Đ$.

**Solution Characterization and Imaging.** *n*-Hexane (HPLC, ≥97%) and *N*,*N*-dimethylacetamide (DMAc, anhydrous, 99.8%) were purchased from Sigma-Aldrich and used as received. To minimize water absorption into DMAc, samples were stirred for 1 h and tested immediately. Dynamic light scattering (DLS) and transmittance measurements were performed on a Litesizer 500 (Anton Paar) with a 658 nm laser in quartz cuvettes with a PTFE stopper (Thorlabs, Inc.). Data analysis was performed with Kalliope software (Anton Paar). Solutions were heated above the cloud point, and the temperature was decreased in 1 °C increments. The temperature was equilibrated for 2 min prior to data collection. Cloud point temperatures ($T_{cp}$) were taken when solution transparency dropped to 10% of the original solution transparency. $R_H$ was measured on ∼1 wt % polymer solutions filtered with Titan3 0.2 μm pore size PTFE filters (Thermo Scientific) at 10 °C above $T_c$. Measurements were performed in triplicate. Particle size dispersity ($D$) was calculated from the DLS measurements by

$$D = \left(\frac{\sigma}{\bar{d}}\right)^2 \quad (1)$$

where $\bar{d}$ is the mean particle diameter and $\sigma$ is the standard deviation of the measured peak.

Transmission electron microscopy (TEM) was performed with a Talos F200X (FEI) at an accelerating voltage of 200 kV. Samples were prepared by precipitating 20 μL drops of 1 wt % micellar solution into 2 mL of deionized (DI) water. The precipitated polymer was stained with 7 μL of 4 wt % $OsO_4$ for 3 h. Samples were centrifuged at 10,000 rpm for 10 min. The top 80% of the solution was removed and replaced with deionized water. This process was repeated 3 times to remove excess $OsO_4$. A 7 μL drop of the stained precipitated polymer was drop-cast onto a 200 mesh copper TEM grid coated with a carbon film (Ted Pella, Inc.) and dried under ambient conditions.


https://doi.org/10.1021/acs.macromol.3c02111
Macromolecules 2024, 57, 916−925

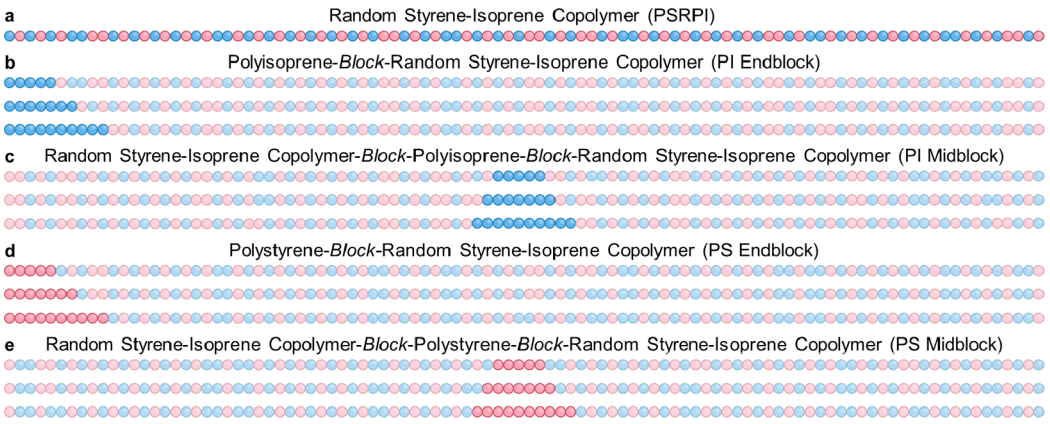


**Figure 1.** (a) Summary of the sequence variations studied here. Random copolymers were synthesized with a 5, 7.5, or 10 kg/mol homopolymer block at the (b,d) end or in the (c,e) middle of the chain.

Micelle stability was tested on a 1 wt % 10K PI end block copolymer in *n*-hexane. DLS measurements were collected at 25 °C directly after the solution. The stoppered cuvette was left undisturbed at ambient conditions for 12 days and retested.

## RESULTS AND DISCUSSION

**Synthesis and Characterization of Copolymers.** Styrene−isoprene copolymers with a similar molecular weight (≈100 kg/mol), molecular weight dispersity ($Đ \approx 1.07$), and overall composition (≈50/50 w/w of styrene/isoprene) but small changes in the monomer sequence were synthesized by anionic polymerization. Anionic polymerization was selected due to the excellent control of block molecular weight, minimal block termination, and low dispersity that it provides. Randomization of the styrene−isoprene sequence within the random block was accomplished by using a solvent mixture of cyclohexane and triethylamine, which has previously been shown[42] to yield random sequences, with no significant down-chain gradient, over a broad range of styrene−isoprene ratios. The sequence of a styrene−isoprene random copolymer chain was altered by placing either a PS or PI homopolymer block at either the end or the center of the otherwise random polymer chain. The molecular weight of the homopolymer block was also varied to be 5, 7.5, or 10 kg/mol. When incorporating a homopolymer block, the composition of the random blocks of the copolymer was adjusted to ensure that the overall chain composition remained at 50/50 w/w styrene/isoprene. A schematic of the sequences of the polymers studied here is shown in Figure 1.

The molecular weight and dispersity were measured by gel permeation chromatography (GPC, Figure S2), and the monomer composition and isoprene microstructure were measured by $^1$H nuclear magnetic resonance (NMR) spectroscopy (Figure S3). The molecular characteristics for each polymer are summarized in Table 1. Each polymer has a low $Đ$ (≤1.13) and negligible termination between blocks (Figure S2). The use of a polar modifier during synthesis substantially increased the content of nonconjugated addition (3,4- and 1,2-addition repeat units) in the PI microstructure.[43] However, by using the same reaction conditions for each polymerization, the 3,4 + 1,2 content was constant across all polymers at ∼47% (Table S1).

**Phase Behavior of Random Copolymers in Selective Solvents.** To account for slight variations in the monomer composition between block−random polymers, the phase behavior of a series of random copolymers (PSRPI) was studied as a baseline. The weight fraction of styrene in these polymers varied from 0.45 to 0.51, and $T_{cp}$ was measured in two solvents: *n*-hexane and DMAc. These solvents were selected because *n*-hexane is a good solvent for PI and a poor solvent for PS,[44] whereas DMAc is a poor solvent for PI and a good solvent for PS.[45] Additionally, $T_{cp}$ values for these two systems were within a convenient experimental window (between 0 °C and the normal boiling point). $T_{cp}$ was measured by turbidimetry; solutions were heated above $T_{cp}$ and slowly cooled. $T_{cp}$ is reported as the temperature at which the solution transparency dropped below 10%.[17] Cloud point transitions were extremely sharp, as transitions occurred within 2 °C. Representative turbidity measurements are shown in Figures S4 and S5. As shown in Figure 2, $T_{cp}$ was measured over a range of solvent/polymer compositions to construct the binodal curves, which are adequately described by the mean-field Flory−Huggins model[15,16,46] (dotted lines, see the SI for details of the calculations and best-fit expressions for $\chi(T)$).

From the binodal curves, $T_c$ was selected as the highest observed $T_{cp}$ for each solvent/polymer system. $T_c$ can then be

**Table 1. Molecular Characteristics of Synthesized Polymers**

| polymer sequence | $M_n$(kg/mol) | $Đ$ | wt % styrene |
|---|---|---|---|
| PSRPI | 109 | 1.06 | 50.7 |
| PSRPI | 112 | 1.07 | 48.7 |
| PSRPI | 121 | 1.07 | 46.0 |
| PSRPI | 107 | 1.06 | 44.5 |
| 5K PI end block | 129 | 1.07 | 50.1 |
| 5K PI end block | 114 | 1.05 | 47.0 |
| 5K PI end block | 133 | 1.07 | 44.9 |
| 7.5K PI end block | 101 | 1.07 | 50.6 |
| 10K PI end block | 137 | 1.06 | 50.1 |
| 5K PI midblock | 112 | 1.07 | 48.0 |
| 7.5K PI midblock | 101 | 1.10 | 49.5 |
| 10K PI midblock | 99 | 1.08 | 47.2 |
| 5K PS end block | 108 | 1.06 | 49.0 |
| 5K PS end block | 136 | 1.13 | 46.8 |
| 5K PS end block | 123 | 1.08 | 44.7 |
| 7.5K PS end block | 146 | 1.08 | 49.8 |
| 10K PS end block | 116 | 1.07 | 49.1 |
| 5K PS midblock | 108 | 1.07 | 47.4 |
| 7.5K PS midblock | 103 | 1.10 | 50.7 |
| 10K PS midblock | 101 | 1.09 | 51.0 |


https://doi.org/10.1021/acs.macromol.3c02111
Macromolecules 2024, 57, 916−925

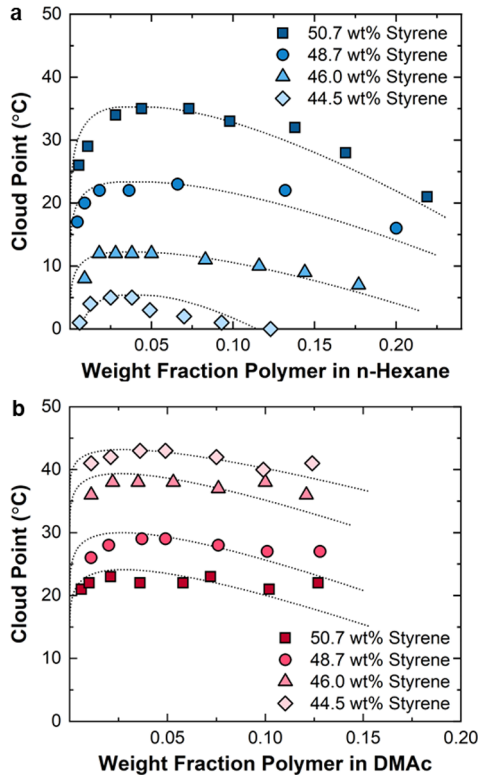


**Figure 2.** Cloud point temperatures for PSRPI copolymers in (a) *n*-hexane and (b) DMAc. Dotted lines are the mean-field Flory–Huggins model using the best-fit expression for $\chi(T)$ for each copolymer.

described as a function of the weight fraction of styrene in the copolymer (Figure 3). As anticipated for the selective solvents,

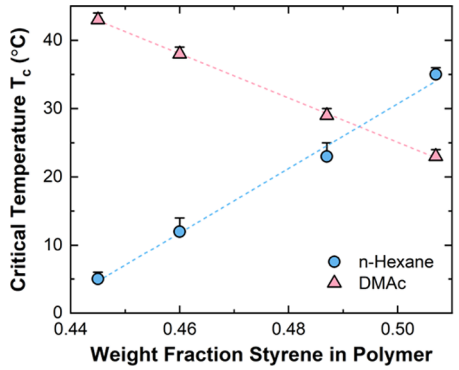


**Figure 3.** $T_c$ of PSRPI copolymers in *n*-hexane (blue circles) and DMAc (pink triangles) as a function of the styrene content. Dashed lines are lines of best fit. Error bars represent the breadth of the transition.

increasing the weight fraction of styrene in the copolymer increases $T_c$ in *n*-hexane and decreases $T_c$ in DMAc. The trend is approximately linear for both solvents over the narrow compositional range explored here. The line of best fit obtained for each solvent system was subsequently used as a baseline against which the $T_c$ for the block–random copolymers was compared. Furthermore, *n*-hexane appears slightly more selective than DMAc, with an absolute average change in $T_c$ of 4.7 °C per 1 wt % change in the composition, compared with a change in $T_c$ of 3.2 °C per 1 wt % in DMAc.

Additionally, DLS was used to measure the hydrodynamic radius ($R_H$) of PSRPI. The measurements were conducted at 1 wt % polymer in solvent at 10 °C above the $T_c$. $R_H$ for all random copolymer unimers in both solvents is ≈12 nm (Figure S8), which falls between the expected $R_H$ for similar molecular weight 1,4-PI (13 nm) and PS (8 nm) in cyclohexane.[47] By obtaining this baseline for unimers in solution, microphase separation (micellization) in block–random copolymers can be observed as a significant increase in $R_H$.

**Phase Behavior of Copolymers with Homopolymer Midblocks.** Block–random copolymers were characterized for both micro- and macrophase separation. $T_c$ values for copolymers with a PI or PS block in the center of a random copolymer chain (Figure 1c,e) were determined by the same procedure as for the random copolymers; $T_{cp}$ was measured at various weight fractions to construct the binodal curve (example diagrams are shown in Figure S9). $T_c$ for each block–random copolymer was then compared (Figure S10) to the $T_c$ expected for a completely random copolymer (Figure 3) with the same overall composition. The shift in $T_c$ is expressed as $\Delta T_c = T_{c,block-random} - T_{c,PSRPI}$. Figure 4 shows $\Delta T_c$ as a function of the targeted $M_n$ of the homopolymer block. Polymers in the two solvent systems show remarkably analogous phase behavior. For solvophobic homopolymer midblocks (PI midblocks in DMAc and PS midblocks in *n*-hexane), $T_c$ decreases with an increasing homopolymer block length (Figure 4a). In these polymers, the solvophobic component is redistributed to the center of the polymer, which, in turn, enriches the random end blocks in the solvophilic component. Furthermore, there is a significant increase in $R_H$ with an increasing solvophobic midblock molecular weight above 5K (Figure 4b). The increase in $R_H$ is due to the formation of starlike micelles prior to macrophase separation. At the conditions studied here, the 7.5K midblock polymers have a mixture of unimers (individualized chains) and micelles in solution, as indicated by a broad peak in the size distribution measured by DLS, whereas the 10K midblock polymers form micelles essentially exclusively (Figure S11). The aggregation number ($N_{agg}$) of the starlike micelles can be estimated by comparing the increase in $R_H$ to that for star polymers as the arm number is increased.[48] By considering a unimer ($R_H \approx 12$ nm) with a solvophobic middle block to be a "2-arm star", $R_H$ (≈26 nm) for the starlike micelles formed by chains with 10K solvophobic midblocks corresponds to a 16-arm star, giving $N_{agg} \approx 8$. The formation of micelles stabilizes the polymer in the solvent prior to macrophase separation, resulting in a large decrease in the $T_c$.

Solvophilic homopolymer midblocks (PI midblocks in *n*-hexane and PS midblocks in DMAc) present the opposite trend: $T_c$ increases with an increasing homopolymer block length (Figure 4c), which progressively enriches the end blocks in the solvophobic component. Unlike systems with a solvophobic midblock, the $R_H$ values for polymers with a solvophilic midblock are not significantly different from those for PSRPI unimers. Therefore, $\Delta T_c$ for these systems does not reflect microphase separation; rather, it indicates that the composition of the ends of the chain has a stronger influence, vs the composition of the middle of the chain on overall compatibility with the solvent.

**Phase Behavior of Copolymers with Homopolymer End Blocks.** Similarly, the phase behavior of copolymers with homopolymer end blocks (Figure 1b,d) was compared with


https://doi.org/10.1021/acs.macromol.3c02111
Macromolecules 2024, 57, 916–925

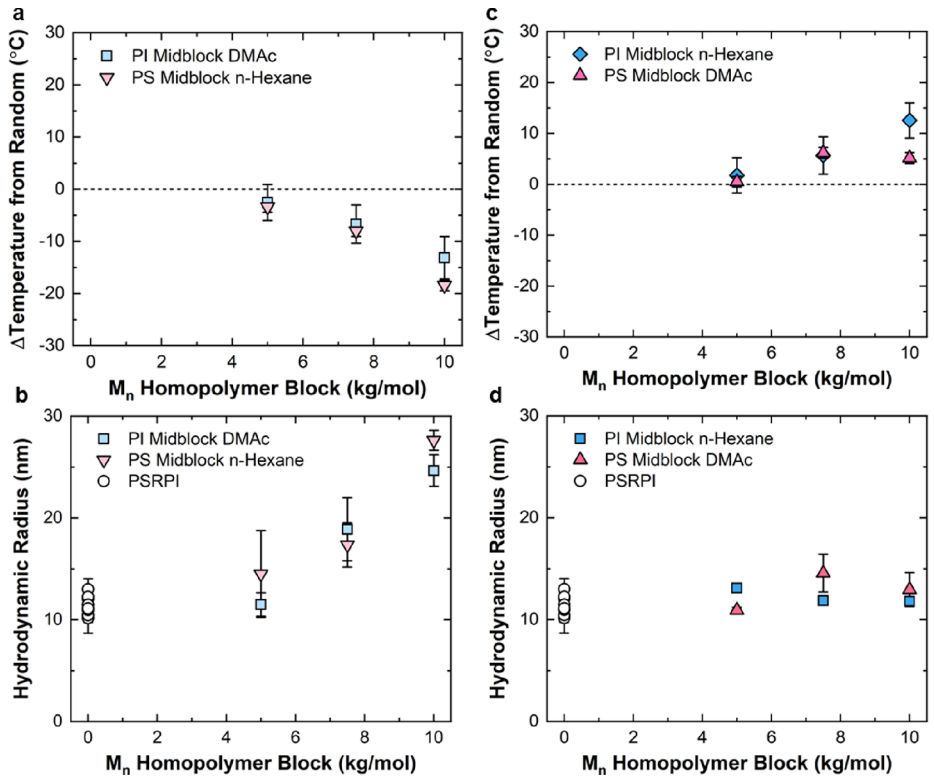


**Figure 4.** Shift in $T_c$ relative to PSRPI copolymers of the same overall composition for (a) polymers with solvophobic homopolymer midblocks and (c) polymers with solvophilic homopolymer midblocks. Error bars are a combination of the uncertainty in the linear fit of the PSRPI copolymer $T_c$ and the uncertainty in the cloud point measurement. $R_H$ for (b) polymers with solvophobic homopolymer midblocks and (d) polymers with solvophilic homopolymer midblocks, measured on 1 wt % solutions at $T_c$ + 10 °C. Error bars are ±1 standard deviation of three experimental replicates.

PSRPI copolymers of the same composition. For polymers with solvophobic homopolymer end blocks, we observe two very different behaviors: polymers with PI end blocks in DMAc show a moderate decrease in $T_c$ with an increasing homopolymer block length, whereas polymers with PS end blocks in *n*-hexane show a very large increase in $T_c$ (Figure 5a). As discussed previously, the ends of the chain have a larger impact on phase behavior than the middle of the chain. However, unlike polymers with homopolymer midblocks, these polymers are architecturally asymmetric: one end of the polymer has favorable polymer/solvent interactions, and the other end has unfavorable interactions. When the two blocks have sufficiently different interactions with the solvent, micellization can occur, which, similar to polymers with a homopolymer midblock, will decrease $T_c$. To demonstrate the impact of slight changes in compatibility between the soluble block and the solvent, polymers with 5K PI end blocks were synthesized at three different overall compositions (Table 1). As shown in Figure 5c,d, when the styrene content in the polymer is low (≤47 wt %), the polymer remains a unimer in solution and $T_c$ is essentially the same as in the PSRPI copolymer case ($\Delta T_c \approx 0$). Conversely, when the overall styrene content is increased above 50 wt %, the random block and PI block in the polymer are sufficiently different in solubility to prompt micellization, as reflected by the large increase in $R_H$ (Figure 5d). For polymers with a 7.5K or 10K PI homopolymer end block, the two ends of the chain have sufficiently different interactions with the solvent, for any styrene weight fraction explored, to prompt micellization ($\Delta T_c < 0$ in Figure 5a). When comparing $R_H$ of the micelles to star polymers, we estimate $N_{agg} \approx 20$ for micelles formed by polymers with PI end blocks in DMAc. For polymers with a PS end block, we do not see the formation of micelles for the composition range studied here (Figure 5b), leading to a positive $\Delta T_c$ (Figure 5a) that increases with the PS block molecular weight, again reflecting the stronger influence of the ends of the chain on compatibility with the solvent.

Likewise, polymers with solvophilic homopolymer end blocks also have architectural asymmetry that prompts either micellization and a decrease in $T_c$ or no micellization and an increase in $T_c$. As shown in Figure 5e,f, polymers with a 7.5K PS end block in DMAc do not form micelles and show a positive $\Delta T_c$, while polymers with a 10K PS end block form very large micelles (discussed further in the following section) and show a negative $\Delta T_c$. On the other hand, polymers with a PI end block form micelles in *n*-hexane at both 7.5K and 10K block sizes, at sufficient polymer concentrations. Note that all the $R_H$ measurements in Figure 5f were taken at 1 wt % polymer, which is slightly below the critical micelle concentration (CMC) for the polymer with the 7.5K PI end block in *n*-hexane; however, micelles form in this system at 2 wt % polymer (Figure S12) and above, including at the critical composition, where $T_c$ (Figure 5e) is determined.

These results compare favorably with coarse-grained molecular simulations, where a 5% change in absolute $T_c$ was calculated by moving a 5 wt % solvophilic block from the middle of a polymer chain to the end of a polymer chain.[38] Experimentally, we obtain a 5% change in $T_c$ when a 7.5 wt % PI block is shifted from the chain end to the middle in *n*-hexane or a 10 wt % PS block is shifted from the chain end to


https://doi.org/10.1021/acs.macromol.3c02111
Macromolecules 2024, 57, 916−925

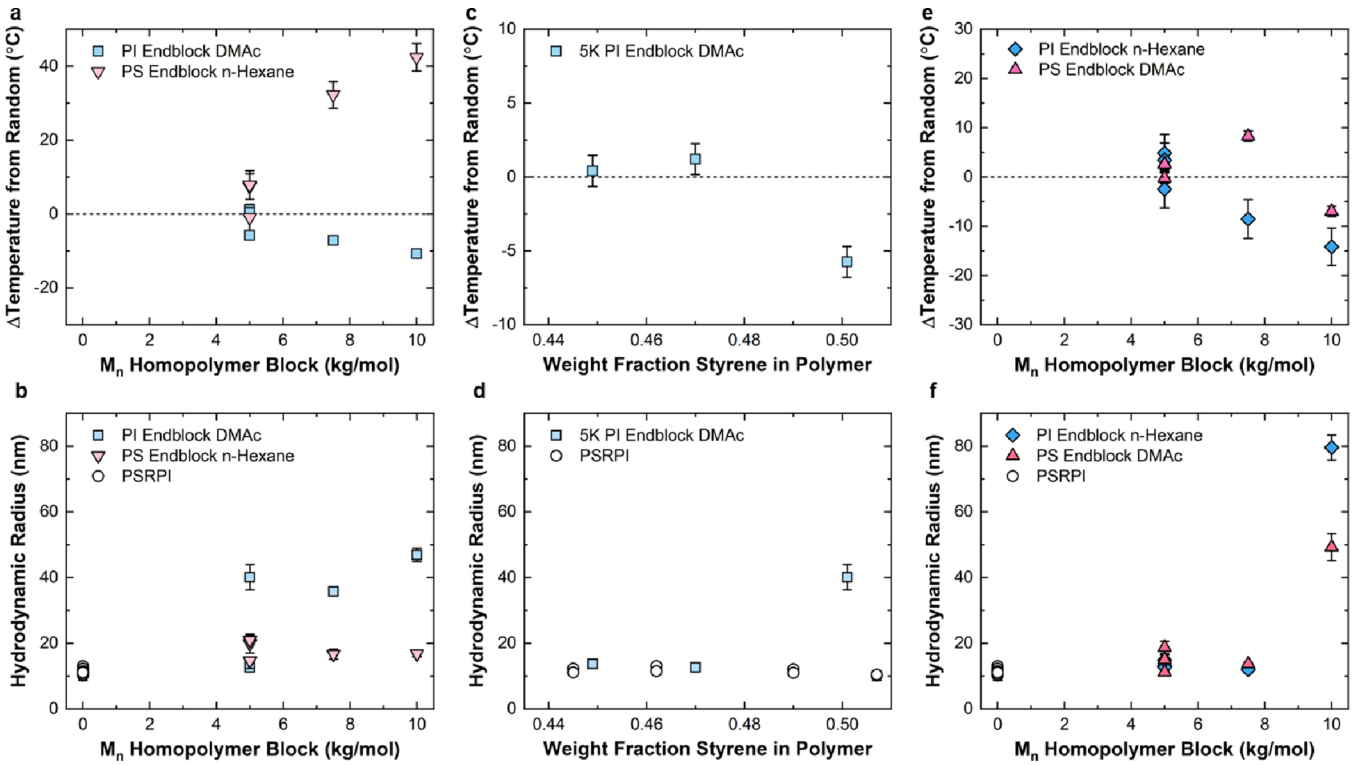


**Figure 5.** Shift in $T_c$ relative to PSRPI copolymers of the same overall composition for (a) polymers with solvophobic homopolymer end blocks, (c) polymers with 5K PI end blocks as a function of the styrene content, and (e) polymers with solvophilic homopolymer end blocks. Error bars are a combination of uncertainty in the linear fit of the PSRPI copolymer $T_c$ and uncertainty in the cloud point measurement. $R_H$ for (b) polymers with solvophobic homopolymer end blocks, (d) polymers with 5K PI end blocks as a function of the styrene content, and (f) polymers with solvophilic homopolymer end blocks measured on 1 wt % solutions at $T_c$ + 10 °C. Error bars are ±1 standard deviation of three experimental replicates.

the middle in DMAc. The quantitative differences (5 vs 7.5 vs 10 wt %) reflect variations in the strengths of the solvophilic/phobic interactions in the three cases.

**Phase Diagram and Thermodynamics of Crew-Cut Micelle Formation.** Crew-cut micelles are formed when the insoluble core-forming block is significantly larger than the soluble corona-forming block, which corresponds to the micelles revealed by DLS in Figure 5f. Previously, polymers with extremely large core-forming blocks could not be dissolved in sufficiently selective solvents;[40,49,50] crew-cut micelles could be prepared only by dissolving the polymer in a good solvent, slowly adding a selective solvent, and dialyzing to remove the good solvent.[40,49,51] The crew-cut micelles that form from polymers with a 10K solvophilic homopolymer block (Figure 5f) are particularly interesting due to their large size ($R_H$ > 50 nm), uniformity (particle size dispersity $D$ < 0.14 by DLS, Figure S12), and formation by direct dissolution. To the best of our knowledge, spontaneous formation of micelles with such a large insoluble, core-forming block (90 wt % of the polymer chain) simply upon the addition of a solvent has not been reported. Here, the crew-cut geometry is made accessible by the use of random copolymerization to carefully tune the interactions so that the core-forming block is not so insoluble that it precipitates but incompatible enough that it becomes thermodynamically favorable to form micelles. Note that the contour lengths of these polymers (~400 nm) are only a fewfold larger than the radii of the crew-cut micelles (~80 nm); to avoid excessive chain stretching, it is likely that the cores of the micelles have "engulfed" some entire polymer chains, rather than having all solvophilic blocks reside in the crew-cut corona.

In addition to the monomodal peak in DLS, the presence of large, uniform micelles can be seen visually by the blue appearance of the solution in reflected light and the orange appearance in transmitted light (Figure S13). As seen in Figure 6, crew-cut micelles can also be observed by isolating them in

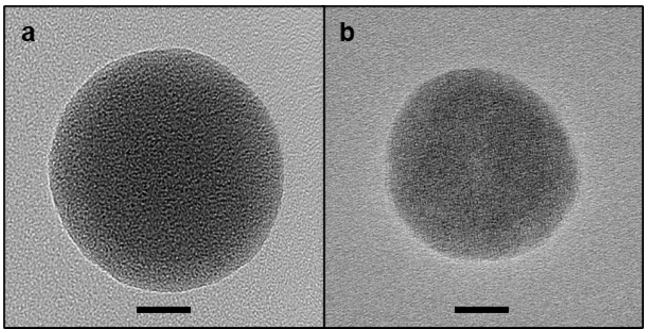


**Figure 6.** TEM images of precipitated and dried crew-cut micelles formed by (a) 10K PI end block polymer in *n*-hexane and (b) 10K PS end block polymer in DMAc. Scale bars: 20 nm.

water, staining with $OsO_4$, and imaging with transmission electron microscopy (TEM). Radius distributions of the crew-cut micelles from TEM for both polymers with 10K end blocks, compared with the distributions from DLS, can be found in Figure S14. The distribution observed by TEM is shifted to slightly smaller radii, as expected for dried micelles compared with micelles suspended in a solvent, but the breadths and shapes of the distributions from both techniques are similar. By assuming that the isolated and dried micelles


https://doi.org/10.1021/acs.macromol.3c02111
Macromolecules 2024, 57, 916−925

measured by TEM are dense polymer spheres, $N_{agg}$ was estimated as 1600 for crew-cut micelles formed by the polymer with a 10K PI end block in *n*-hexane and 1000 for crew-cut micelles formed by the polymer with a 10K PS end block in DMAc. The large $N_{agg}$ for the crew-cut micelles (~1000) compared with that for starlike micelles (~20) formed by the same polymer (10K PI end block in *n*-hexane vs DMAc) shows the remarkable difference in structure between the two different types of spherical micelles.

Furthermore, the kinetic stability of the crew-cut micelles was tested. $R_H$ for the crew-cut micelles formed by the 10K PI end block polymer in *n*-hexane was measured by DLS directly after the polymer was fully dissolved. The sample was left undisturbed at room temperature for 12 days and measured again; $R_H$ did not change significantly (Figure S15a). Micelle formation is also thermoreversible: solutions that form crew-cut micelles at room temperature can be heated above the critical micelle temperature ($T_{CMT}$) to form unimers and then cooled to room temperature to reform micelles with the same average size and distribution (Figure S15b).

The ability for polymers to both micro- and macrophase-separate was previously considered to be a unique property of aqueous systems,[25] with molecular simulations only recently indicating that this behavior should be achievable in other solvents.[26] Here, we experimentally define a phase diagram of microphase separation into crew-cut micelles and macrophase separation into unimer and concentrated micelle phases that is obtainable by delicate tuning of the solvent/block compatibilities. Furthermore, the phase diagram can provide insights into the thermodynamics of micellization of these large crew-cut micelles compared with traditional starlike micelles. At high temperatures at all concentrations, the polymers are fully dissolved, existing as unimers in solution (blue regions in Figure 7). At high polymer concentrations (>0.3 wt % 10K PI end block polymer in *n*-hexane and >0.07 wt % 10K PS end block polymer in DMAC, to the right of the vertical dotted black lines), as the solutions are cooled, the random block becomes incompatible with the solvent resulting in the formation of crew-cut micelles. In Figure 7, the CMC as a function of temperature is shown as a purple dashed line, and the purple area below that line represents temperatures and compositions that form a macroscopically single-phase micellar solution. Using the experimentally determined CMC vs temperature ($T_{CMT}$) curve, the Gibbs free energy of micellization ($\Delta G^\circ_{mic}$), enthalpy of micellization ($\Delta H^\circ_{mic}$), and entropy of micellization ($\Delta S^\circ_{mic}$) can be calculated using the following relationships, wherein the CMC is expressed as a mole fraction of polymer chains:[52]

$$\Delta G^\circ_{mic} = RT_{CMT}\ln \text{CMC} \tag{2}$$

$$\Delta H^\circ_{mic} = R\frac{d(\ln \text{CMC})}{d(1/T_{CMT})} \tag{3}$$

$$\Delta S^\circ_{mic} = \frac{\Delta H^\circ_{mic} - \Delta G^\circ_{mic}}{T_{CMT}} \tag{4}$$

$\Delta G^\circ_{mic}$ ranges from −35 to −25 kJ/mol for both polymer/solvent systems (Figure S16). The value of $\Delta G^\circ_{mic}$ is similar to that for block copolymers forming starlike micelles in organic,[45,53,54] ionic,[55] and aqueous[56,57] solvents despite having a drastically different aggregation number and micellar structure, as it must be, since ln CMC across systems with an

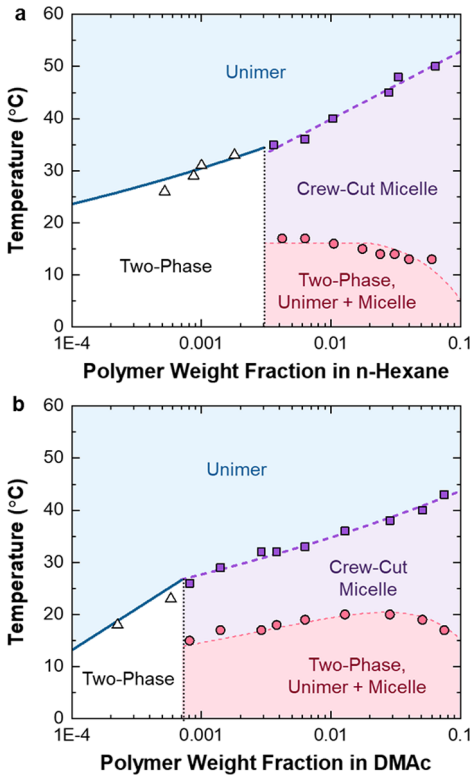


**Figure 7.** Phase behavior of (a) 10K PI end block polymer in *n*-hexane and (b) 10K PS end block polymer in DMAc as a function of temperature and polymer weight fraction. The blue region indicates conditions under which the polymer is individualized in solution (unimers). The dashed purple line indicates the CMC. The purple region indicates conditions where the polymer forms crew-cut micelles that are uniformly dispersed. The pink dashed line marks the boundary below which a polymer-rich micellar phase and a polymer-poor unimer phase coexist. The white region at a low concentration represents when macrophase separation occurs prior to micellization.

accessible CMC varies only modestly. Furthermore, $\Delta S^\circ_{mic}$ for both systems is negative (Figure S16), and $\Delta H^\circ_{mic}$ (Figure S17) is large and negative. Unlike aqueous starlike micelles that are entropically favorable due to the favorable release of water molecules to the bulk solution, the self-assembly seen here is enthalpy-driven:[45] unfavorable solvent/polymer segmental interactions are shielded by forming a dense polymer core in the micelle. The core-forming block is very large, resulting in a large molar $\Delta H^\circ_{mic}$ (−144 kJ/mol for the 10K PI end block copolymer in *n*-hexane and −232 kJ/mol for the 10K PS end block in DMAc), which is in line with previous values determined for starlike micelles in DMAc and hydrocarbons when normalized for the core block length, despite the large differences in the micelle structure.[45,53,54,58] The enthalpic gain is sufficiently large to overcome the entropic penalty from the reduction in the translational freedom of the polymer chains when they micellize.

If the high-concentration micellar solutions are cooled further, macrophase separation occurs (dark pink region in Figure 7), resulting in a top phase containing dilute unimers and a bottom phase containing concentrated micelles (photograph in Figure S13b). At sufficiently low polymer concentrations (to the left of the vertical dotted black lines in Figure 7), there is no single-phase micellar solution, and the boundary


https://doi.org/10.1021/acs.macromol.3c02111
Macromolecules 2024, 57, 916−925

defining the unimer region exhibits a change in the slope. These changes occur because the CMC dips below the Flory–Huggins binodal at the polymer volume fraction corresponding to the vertical dotted black line (Figure S18). Therefore, when the polymer solution is cooled, it transitions directly from unimers to a two-phase solution, where the polymer-rich phase contains micelles and the polymer-poor phase contains unimers (white region in Figure 7). The polymer-rich phase, which has a polymer weight fraction of >0.1, is sufficiently concentrated that crew-cut micelles form, as evidenced by the opalescent appearance of the concentrated phase. However, since the formation of these micelles proceeds simultaneously with macrophase separation and the polymer-rich phase is highly viscous, these micelles may not have the same size as those formed from a solution with a slightly higher overall polymer concentration (to the right of the dotted black vertical line), where upon cooling, micellization proceeds first through a uniform phase of crew-cut micelles and only subsequently separates to yield a concentrated phase of micelles. Furthermore, the macrophase separation exhibited by solutions to the left of the dotted black vertical line kinetically thwarts the formation of a uniform phase of crew-cut micelles; once the solution has split into two macroscopic phases, resuspension of micelles into a uniform phase would be an extremely slow process, even if thermodynamically favored.

A summary of the observed phase behavior as a function of the interaction parameter ($\chi$) between the homopolymer block and the solvent and the random copolymer block and the solvent is shown in Figure 8. The critical $\chi$ ($\chi_c$) for each block is shown by the dotted black lines. Equal compatibility between each block and the solvent (i.e., when the polymer is completely random) is shown by the black dashed line. For polymers with either solvophobic end blocks or midblocks, starlike micelles will form when the homopolymer block is suitably incompatible with the solvent ($\chi$ sufficiently greater than $\chi_c$) and the random block is suitably compatible ($\chi$ sufficiently below $\chi_c$). This region is colored purple in the top left corner of the phase diagram. When the homopolymer block is solvophilic, the phase behavior of end block- and midblock-containing polymers differs, with regard to the presence or absence of a region of crew-cut micelles. A polymer with a solvophilic end block can form crew-cut micelles, though over only a narrow interaction range; this narrowness reflects the fact that $\chi$ between the large random block and the solvent must not be substantially greater than $\chi_c$, or the polymer simply macrophase-separates. By contrast, crew-cut micelle formation was not observed for solvophilic midblock copolymers. In this case, the solvophilic midblock would need to loop to form the crew-cut structure, which would be entropically unfavorable. Therefore, the bottom right of the phase diagram for midblock-containing polymers does not show any microphase separation.

## CONCLUSIONS

In this study, styrene–isoprene copolymers were synthesized with small variations in the monomer sequence, which nevertheless exert substantial control over the phase behavior. By designing systems that can microphase-separate, the polymer becomes more stable in solution, and $T_c$ is reduced. In contrast, by decreasing the compatibility between the ends of the polymer chain and the solvent without promoting microphase separation, $T_c$ is elevated. Furthermore, the experimental results observed here align closely with coarse-grained molecular simulations.[38] Both results indicate that the ends of a polymer chain have a larger impact on the phase behavior than the units at the center of a chain and that small changes in the sequence (5–10 wt %) can modulate absolute $T_c$ by 5%. Finally, we demonstrate an enthalpically driven system that can both micro- and macrophase-separate by changing thermodynamic conditions. By carefully tuning solvent/polymer interactions, large ($N_{agg}$, ~1000) crew-cut micelles form spontaneously at room temperature and can macrophase-separate into a dilute unimer phase and a concentrated micelle phase upon cooling. These insights can be used to engineer new thermoresponsive systems that have improved control over micro- and macrophase separation for the development of new smart materials for healthcare and environmental applications.

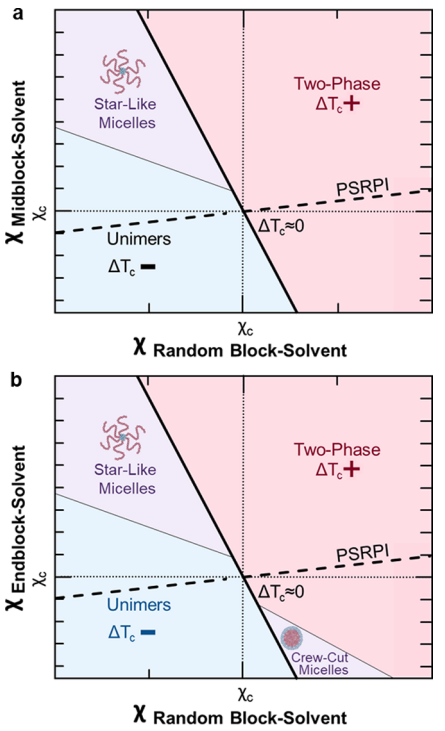


**Figure 8.** Summary of the observed phase behavior for polymers with (a) a homopolymer midblock and (b) a homopolymer end block. Diagrams correspond to a fixed homopolymer:random copolymer block ratio (e.g., 5:1:5 for the midblock and 1:10 for the end block) and a polymer concentration equal to $\Phi_{P,c}$(≈3 wt % here). $\chi_c$ represents the critical value of the interaction parameter (≈0.53 here, see Figures S6 and S7); note that the *y*-axis scale spans a much greater range of $\chi$ than the *x*-axis scale.

## ASSOCIATED CONTENT

### Supporting Information

The Supporting Information is available free of charge at https://pubs.acs.org/doi/10.1021/acs.macromol.3c02111.

Synthesis schematics, table of PI microstructures, GPC traces, $^1$H NMR spectra, turbidmetry measurements, Flory interaction parameters for random copolymers, binodal phase diagrams, DLS distributions, hydrodynamic radius as a function of the molecular weight and styrene content, micelle size distribution from TEM and DLS, photograph of macrophase separation, Gibbs free energy and entropy of micellization, enthalpy of



https://doi.org/10.1021/acs.macromol.3c02111
Macromolecules 2024, 57, 916–925

micelle formation, and phase behavior of crew-cut micelles (PDF)

## AUTHOR INFORMATION


### Corresponding Authors

**Rodney D. Priestley** − *Department of Chemical and Biological Engineering, Princeton Materials Institute, Princeton University, Princeton, New Jersey 08544, United States;* orcid.org/0000-0001-6765-2933; Email: rpriestl@princeton.edu

**Richard A. Register** − *Department of Chemical and Biological Engineering, Princeton Materials Institute, Princeton University, Princeton, New Jersey 08544, United States;* orcid.org/0000-0002-5223-4306; Email: register@princeton.edu

### Author

**Lauren W. Taylor** − *Department of Chemical and Biological Engineering, Princeton Materials Institute, Princeton University, Princeton, New Jersey 08544, United States;* orcid.org/0000-0002-6497-2795

Complete contact information is available at: https://pubs.acs.org/10.1021/acs.macromol.3c02111


### Notes

The authors declare no competing financial interest.

## ACKNOWLEDGMENTS

This work was generously supported by the National Science Foundation Materials Research Science and Engineering Center (NSF MRSEC) Program, through the Princeton Center for Complex Materials (DMR-2011750). We acknowledge the use of Princeton's Imaging and Analysis Center (IAC), which is also partially supported by the Princeton Center for Complex Materials. We would like to thank Athanassios Z. Panagiotopoulos for stimulating discussions.

## REFERENCES


(1) Wienk, I. M.; Boom, R. M.; Beerlage, M. A. M.; Bulte, A. M. W.; Smolders, C. A.; Strathmann, H. Recent Advances in the Formation of Phase Inversion Membranes Made from Amorphous or Semi-Crystalline Polymers. *J. Membr. Sci.* **1996**, *113* (2), 361−371.

(2) Grundy, L. S.; Lee, V. E.; Li, N.; Sosa, C.; Mulhearn, W. D.; Liu, R.; Register, R. A.; Nikoubashman, A.; Prud'homme, R. K.; Panagiotopoulos, A. Z.; Priestley, R. D. Rapid Production of Internally Structured Colloids by Flash Nanoprecipitation of Block Copolymer Blends. *ACS Nano* **2018**, *12* (5), 4660−4668.

(3) Liu, J. X.; Bizmark, N.; Scott, D. M.; Register, R. A.; Haataja, M. P.; Datta, S. S.; Arnold, C. B.; Priestley, R. D. Evolution of Polymer Colloid Structure During Precipitation and Phase Separation. *JACS Au* **2021**, *1* (7), 936−944.

(4) Feric, M.; Vaidya, N.; Harmon, T. S.; Mitrea, D. M.; Zhu, L.; Richardson, T. M.; Kriwacki, R. W.; Pappu, R. V.; Brangwynne, C. P. Coexisting Liquid Phases Underlie Nucleolar Subcompartments. *Cell* **2016**, *165* (7), 1686−1697.

(5) Shin, Y.; Brangwynne, C. P. Liquid Phase Condensation in Cell Physiology and Disease. *Science* **2017**, *357* (6357), No. eaaf4382.

(6) Riback, J. A.; Katanski, C. D.; Kear-Scott, J. L.; Pilipenko, E. V.; Rojek, A. E.; Sosnick, T. R.; Drummond, D. A. Stress-Triggered Phase Separation Is an Adaptive, Evolutionarily Tuned Response. *Cell* **2017**, *168* (6), 1028−1040.

(7) Zhang, Y.; Furyk, S.; Bergbreiter, D. E.; Cremer, P. S. Specific Ion Effects on the Water Solubility of Macromolecules: PNIPAM and the Hofmeister Series. *J. Am. Chem. Soc.* **2005**, *127* (41), 14505−14510.

(8) Alexandridis, P.; Holzwarth, J. F. Differential Scanning Calorimetry Investigation of the Effect of Salts on Aqueous Solution Properties of an Amphiphilic Block Copolymer (Poloxamer). *Langmuir* **1997**, *13* (23), 6074−6082.

(9) Ikeuchi, N.; Komachi, T.; Murayama, K.; Asanuma, H.; Maruyama, A.; Shimada, N. Light-Regulated Liquid−Liquid Phase Separation for Spatiotemporal Protein Recruitment and Cell Aggregation. *ACS Appl. Mater. Interfaces* **2021**, *13* (4), 5652−5659.

(10) Plamper, F. A.; Ballauff, M.; Müller, A. H. E. Tuning the Thermoresponsiveness of Weak Polyelectrolytes by PH and Light: Lower and Upper Critical-Solution Temperature of Poly(N,N-Dimethylaminoethyl Methacrylate). *J. Am. Chem. Soc.* **2007**, *129* (47), 14538−14539.

(11) Xu, X.; Bizmark, N.; Christie, K. S. S.; Datta, S. S.; Ren, Z. J.; Priestley, R. D. Thermoresponsive Polymers for Water Treatment and Collection. *Macromolecules* **2022**, *55* (6), 1894−1909.

(12) Schmaljohann, D. Thermo- and PH-Responsive Polymers in Drug Delivery. *Adv. Drug Delivery Rev.* **2006**, *58* (15), 1655−1670.

(13) Sponchioni, M.; Capasso Palmiero, U.; Moscatelli, D. Thermo-Responsive Polymers: Applications of Smart Materials in Drug Delivery and Tissue Engineering. *Mater. Sci. Eng., C* **2019**, *102*, 589−605.

(14) Roy, D.; Brooks, W. L. A.; Sumerlin, B. S. New Directions in Thermoresponsive Polymers. *Chem. Soc. Rev.* **2013**, *42* (17), 7214−7243.

(15) Huggins, M. L. Theory of Solutions of High Polymers. *J. Am. Chem. Soc.* **1942**, *64* (7), 1712−1719.

(16) Flory, P. J. Thermodynamics of High Polymer Solutions. *J. Chem. Phys.* **1942**, *10* (1), 51−61.

(17) Aseyev, V.; Tenhu, H.; Winnik, F. M. Non-Ionic Thermoresponsive Polymers in Water. In *Self Organized Nanostructures of Amphiphilic Block Copolymers II*; Müller, A. H. E., Borisov, O., Eds.; Advances in Polymer Science; Springer: Berlin, Heidelberg, 2011; pp 29−89. DOI: 10.1007/12_2010_57.

(18) Rodriguez, F.; Cohen, C.; Ober, C. K.; Archer, L. *Principles of Polymer Systems*, 5th ed.; CRC Press: Boca Raton, 2003 DOI: 10.1201/b12837.

(19) Mai, Y.; Eisenberg, A. Self-Assembly of Block Copolymers. *Chem. Soc. Rev.* **2012**, *41* (18), 5969−5985.

(20) Bates, F. S.; Fredrickson, G. H. Block Copolymer Thermodynamics: Theory and Experiment. *Annu. Rev. Phys. Chem.* **1990**, *41* (1), 525−557.

(21) Topel, Ö.; Çakır, B. A.; Budama, L.; Hoda, N. Determination of Critical Micelle Concentration of Polybutadiene-Block-Poly(Ethyleneoxide) Diblock Copolymer by Fluorescence Spectroscopy and Dynamic Light Scattering. *J. Mol. Liq.* **2013**, *177*, 40−43.

(22) Linse, P. Phase Behavior of Poly(Ethylene Oxide)-Poly(Propylene Oxide) Block Copolymers in Aqueous Solution. *J. Phys. Chem.* **1993**, *97* (51), 13896−13902.

(23) Kositza, M. J.; Bohne, C.; Alexandridis, P.; Hatton, T. A.; Holzwarth, J. F. Dynamics of Micro- and Macrophase Separation of Amphiphilic Block-Copolymers in Aqueous Solution. *Macromolecules* **1999**, *32* (17), 5539−5551.

(24) Cui, S.; Yu, L.; Ding, J. Thermogelling of Amphiphilic Block Copolymers in Water: ABA Type versus AB or BAB Type. *Macromolecules* **2019**, *52* (10), 3697−3715.

(25) Panagiotopoulos, A. Z.; Floriano, M. A.; Kumar, S. K. Micellization and Phase Separation of Diblock and Triblock Model Surfactants. *Langmuir* **2002**, *18* (7), 2940−2948.

(26) Panagiotopoulos, A. Z. Phase Separation and Aggregation in Multiblock Chains. *J. Chem. Phys.* **2023**, *158* (15), 154901.

(27) Liu, P.; Xiang, L.; Tan, Q.; Tang, H.; Zhang, H. Steric Hindrance Effect on Thermoresponsive Behaviors of Pyrrolidone-Based Polymers. *Polym. Chem.* **2013**, *4* (4), 1068−1076.

(28) Huang, X.; Du, F.; Ju, R.; Li, Z. Novel Acid-Labile, Thermoresponsive Poly(Methacrylamide)s with Pendent Ortho Ester Moieties. *Macromol. Rapid Commun.* **2007**, *28* (5), 597−603.

(29) Ward, M. A.; Georgiou, T. K. Thermoresponsive Terpolymers Based on Methacrylate Monomers: Effect of Architecture and

Composition. *J. Polym. Sci., Part A: Polym. Chem.* **2010**, *48* (4), 775−783.
(30) Warne, N. M.; Finnegan, J. R.; Feeney, O. M.; Kempe, K. Using 2-Isopropyl-2-Oxazine to Explore the Effect of Monomer Distribution and Polymer Architecture on the Thermoresponsive Behavior of Copolymers. *J. Polym. Sci.* **2021**, *59* (22), 2783−2796.
(31) Okada, M.; Numasawa, N. Phase Equilibrium of a Star-Shaped Polymer Solution. *Comput. Theor. Polym. Sci.* **1998**, *8* (3), 259−263.
(32) Akiyama, Y.; Shinohara, Y.; Hasegawa, Y.; Kikuchi, A.; Okano, T. Preparation of Novel Acrylamide-Based Thermoresponsive Polymer Analogues and Their Application as Thermoresponsive Chromatographic Matrices. *J. Polym. Sci., Part A: Polym. Chem.* **2008**, *46* (16), 5471−5482.
(33) Inoue, S.; Kakikawa, H.; Nakadan, N.; Imabayashi, S.; Watanabe, M. Thermal Response of Poly(Ethoxyethyl Glycidyl Ether) Grafted on Gold Surfaces Probed on the Basis of Temperature-Dependent Water Wettability. *Langmuir* **2009**, *25* (5), 2837−2841.
(34) Gouveia, B.; Kim, Y.; Shaevitz, J. W.; Petry, S.; Stone, H. A.; Brangwynne, C. P. Capillary Forces Generated by Biomolecular Condensates. *Nature* **2022**, *609* (7926), 255−264.
(35) Bracha, D.; Walls, M. T.; Wei, M.-T.; Zhu, L.; Kurian, M.; Avalos, J. L.; Toettcher, J. E.; Brangwynne, C. P. Mapping Local and Global Liquid Phase Behavior in Living Cells Using Photo-Oligomerizable Seeds. *Cell* **2018**, *175* (6), 1467−1480.e13.
(36) Shibata, K.; Kametani, Y.; Daito, Y.; Ouchi, M. Homopolymer-Block-Alternating Copolymers Composed of Acrylamide Units: Design of Transformable Divinyl Monomers and Sequence-Specific Thermoresponsive Properties. *J. Am. Chem. Soc.* **2022**, *144* (22), 9959−9970.
(37) Rana, U.; Brangwynne, C. P.; Panagiotopoulos, A. Z. Phase Separation vs Aggregation Behavior for Model Disordered Proteins. *J. Chem. Phys.* **2021**, *155* (12), 125101.
(38) Statt, A.; Casademunt, H.; Brangwynne, C. P.; Panagiotopoulos, A. Z. Model for Disordered Proteins with Strongly Sequence-Dependent Liquid Phase Behavior. *J. Chem. Phys.* **2020**, *152* (7), No. 075101.
(39) Hazra, M. K.; Levy, Y. Biophysics of Phase Separation of Disordered Proteins Is Governed by Balance between Short- And Long-Range Interactions. *J. Phys. Chem. B* **2021**, *125* (9), 2202−2211.
(40) Zhang, L.; Eisenberg, A. Multiple Morphologies and Characteristics of "Crew-Cut" Micelle-like Aggregates of Polystyrene-b-Poly(Acrylic Acid) Diblock Copolymers in Aqueous Solutions. *J. Am. Chem. Soc.* **1996**, *118* (13), 3168−3181.
(41) Gao, Z.; Varshney, S. K.; Wong, S.; Eisenberg, A. Block Copolymer "Crew-Cut" Micelles in Water. *Macromolecules* **1994**, *27* (26), 7923−7927.
(42) Beckingham, B. S.; Register, R. A. Synthesis and Phase Behavior of Block-Random Copolymers of Styrene and Hydrogenated Isoprene. *Macromolecules* **2011**, *44* (11), 4313−4319.
(43) Kim, J. M.; Chakrapani, S. B.; Beckingham, B. S. Tuning Compositional Drift in the Anionic Copolymerization of Styrene and Isoprene. *Macromolecules* **2020**, *53* (10), 3814−3821.
(44) Hinestrosa, J. P.; Alonzo, J.; Osa, M.; Kilbey, S. M. I. Solution Behavior of Polystyrene−Polyisoprene Miktoarm Block Copolymers in a Selective Solvent for Polyisoprene. *Macromolecules* **2010**, *43* (17), 7294−7304.
(45) Price, C.; Booth, C.; Canham, P. A.; Naylor, T. de V.; Stubbersfield, R. B. The Thermodynamics of Micelle Formation by a Polystyrene-b-Polyisoprene Block Copolymer in N,N′-Dimethylacetamide. *Br. Polym. J.* **1984**, *16* (4), 311−313.
(46) Huggins, M. L. Some Properties of Solutions of Long-Chain Compounds. *J. Phys. Chem.* **1942**, *46* (1), 151−158.
(47) Fetters, L. J.; Hadjichristidis, N.; Lindner, J. S.; Mays, J. W. Molecular Weight Dependence of Hydrodynamic and Thermodynamic Properties for Well-Defined Linear Polymers in Solution. *J. Phys. Chem. Ref. Data* **1994**, *23* (4), 619−640.
(48) Grest, G. S.; Fetters, L. J.; Huang, J. S.; Richter, D. Star Polymers: Experiment, Theory, and Simulation. *Adv. Chem. Phys.* **1996**, *94*, 67−163.
(49) Loos, K.; Böker, A.; Zettl, H.; Zhang, M.; Krausch, G.; Müller, A. H. E. Micellar Aggregates of Amylose-Block-Polystyrene Rod−Coil Block Copolymers in Water and THF. *Macromolecules* **2005**, *38* (3), 873−879.
(50) Zhulina, E. B.; Adam, M.; LaRue, I.; Sheiko, S. S.; Rubinstein, M. Diblock Copolymer Micelles in a Dilute Solution. *Macromolecules* **2005**, *38* (12), 5330−5351.
(51) Cameron, N. S.; Corbierre, M. K.; Eisenberg, A. 1998 E.W.R. Steacie Award Lecture Asymmetric Amphiphilic Block Copolymers in Solution: A Morphological Wonderland. *Can. J. Chem.* **1999**, *77* (8), 1311−1326.
(52) Berg, J. C. *Introduction To Interfaces And Colloids: The Bridge To Nanoscience*; World Scientific Publishing Co.: Hackensack, NJ, Singapore; 2009 DOI: 10.1142/9789814293082_0001.
(53) Price, C.; Stubbersfield, R. B.; El-Kafrawy, S.; Kendall, K. D. Thermodynamics of Micellization of Poly-Styrene-Block-Poly-(Ethylene/Propylene) Copolymers in Decane. *Br. Polym. J.* **1989**, *21* (5), 391−394.
(54) Quintana, J. R.; Villacampa, M.; Munoz, M.; Andrio, A.; Katime, I. A. Micellization of a Polystyrene-Block-Poly(Ethylene/Propylene) Copolymer in n-Alkanes. 1. Thermodynamic Study. *Macromolecules* **1992**, *25* (12), 3125−3128.
(55) Hoarfrost, M. L.; Lodge, T. P. Effects of Solvent Quality and Degree of Polymerization on the Critical Micelle Temperature of Poly(Ethylene Oxide-b-n-Butyl Methacrylate) in Ionic Liquids. *Macromolecules* **2014**, *47* (4), 1455−1461.
(56) Meguro, K.; Takasawa, Y.; Kawahashi, N.; Tabata, Y.; Ueno, M. Micellar Properties of a Series of Octaethyleneglycol-n-Alkyl Ethers with Homogeneous Ethylene Oxide Chain and Their Temperature Dependence. *J. Colloid Interface Sci.* **1981**, *83* (1), 50−56.
(57) Alexandridis, P.; Holzwarth, J. F.; Hatton, T. A. Micellization of Poly(Ethylene Oxide)-Poly(Propylene Oxide)-Poly(Ethylene Oxide) Triblock Copolymers in Aqueous Solutions: Thermodynamics of Copolymer Association. *Macromolecules* **1994**, *27* (9), 2414−2425.
(58) Price, C.; Chan, E. K. M.; Stubbersfield, R. B. The Effect of Block Length on the Thermodynamic Stability of Micelles Formed by Polystyrene-Block-Polyisoprene Copolymers in n-Hexadecane. *Eur. Polym. J.* **1987**, *23* (8), 649−651.